SHEAR-CRITICAL R/C COLUMNS

UNDER INCREASING AXIAL LOAD

Dimitrios K. Zimos, Vassilis K. Papanikolaou, Andreas J. Kappos and Panagiotis E. Mergos

Biography: **Dimitrios K. Zimos** works as a Structural Engineer at the Structural Safety Department of Basler & Hofmann, Zurich. He received his Master's in Civil Engineering from the Aristotle University of Thessaloniki (AUTh) and his PhD in Structural Engineering from City, University of London. His research interests include design and assessment of R/C structures, earthquake engineering and passive structural control.

Vassilis K. Papanikolaou is an Assistant Professor at the School of Civil Engineering, AUTh, Greece. He received his MSc degree from Imperial College, London and his PhD from AUTh. His research interests include analysis of reinforced concrete and masonry structures, finite elements and material constitutive models, computational engineering and programming, experimental methods on new and existing structures and applications of electronics in earthquake engineering and structural monitoring.

Andreas Kappos is a Professor at the Department of Civil Infrastructure & Environmental Engineering at Khalifa University, Abu Dhabi; until 2019 he held appointments at City, University of London and AUTh. He has long worked in the field of Earthquake Structural Engineering, in particular analysis procedures for reinforced concrete buildings and bridges subjected to earthquake loading, and developed several methods and models for seismic assessment of these structures, as well as design procedures based on the use of modern analysis tools.

Panagiotis E. Mergos is a lecturer at City, University of London. He received MSc degrees from AUTh and the University of Pavia, Italy, and his PhD from AUTh. His research

interests include design and assessment of reinforced concrete structures, finite element analysis, earthquake engineering and structural optimization.

SYNOPSIS

Structural elements in old reinforced concrete (R/C) frame buildings are often prone to shear or flexure-shear failure, which can eventually lead to loss of axial load capacity of vertical elements and initiate vertical progressive collapse of a building.

An experimental investigation of shear and flexure-shear critical R/C elements subjected to increasing axial load is reported herein. The focus is on the effect of vertical load redistribution from axially failing columns on the non-linear (pre- and post-peak) response of neighboring shear-dominated members. The test results along with an analysis of the recorded deformation, strength, stiffness and energy dissipation characteristics shed light on the performance of sub-standard columns under constant and increasing axial load subsequent, or just prior, to failing in shear, thus providing useful insights into the assessment of existing R/C structures.

Keywords: Existing structures; Experimental program; Reinforced concrete columns; Shear failure; Axial failure; Vertical load redistribution; Progressive collapse

INTRODUCTION

Many existing reinforced concrete structures have been designed according to older, less demanding, seismic codes or might not have been designed to withstand seismic loads at all. Transverse reinforcement in their structural elements is typically low, widely spaced and/or poorly anchored, rendering them vulnerable to shear failure, subsequent, or even prior, to yielding of their longitudinal reinforcement. Shear failure can eventually lead to loss of axial

load capacity of vertical elements, through disintegration of the poorly confined concrete core[1]. Loss of column axial capacity emerges from post-earthquake reconnaissance as one of the most common reasons of vertical progressive collapse of older R/C frame buildings[2]. Such a column failure means that the vertical loads previously carried by a failing member are subsequently redistributed to neighboring vertical elements. Therefore, the ability of a framing system to resist progressive collapse in such a 'scenario' depends on both the ability of horizontal elements to transfer the loads being redistributed to adjacent vertical elements and the latter's ability to resist them without significant reduction in their strength and deformation capacity[3]. Several numerical and experimental studies, as well as field investigations, have focused on the capacity of horizontal elements to redistribute vertical loads (e.g. [4–7]). The General Services Administration Guidelines[8] also focus on load redistribution systems of gravity loads to neighboring vertical load-bearing elements. Nevertheless, existing research work has not yet concentrated adequately on the vertical members adjacent to an axially failing column; when an abrupt increase of axial load occurs, the capacity to resist progressive collapse should be carefully assessed[9] . This effect has been given only limited consideration in the study of older R/C buildings (e.g. in [10]), without a rigorous treatment of post-peak response. In flexure-critical elements axial load increase can be included by accounting for axial-flexure interaction. However, this is not the case for shear- or flexure-shear-critical elements modeled with beam-column elements explicitly accounting for shear deformations, wherein axial load increase has not yet been modeled. A common assumption in progressive collapse assessment is that of undamaged vertical elements; this may be appropriate for blast-induced or similar collapse scenarios, with damage largely localized in a single element or a small set of elements. Nevertheless, earthquake-induced collapse scenarios pose a further difficulty when there is global damage

in a large part of, if not the entire, building, even before the loss of a column's axial capacity. Therefore, the damage state of a column neighboring an axially failed vertical member has to be appropriately addressed in earthquake-induced progressive collapse assessment (e.g. [10]). Previous experimental studies looking into the non-linear, especially the post-peak, lateral response of shear-critical R/C columns have looked extensively at the response under constant axial load (e.g. [11,12], among several others) and axial load proportional to the lateral force acting on the column (e.g. [1,12,13]). Recently, Nakamura & Yoshimura[14] studied experimentally the effect of decreasing axial load on the non-linear seismic response of shear-critical columns, simulating the response of a column that starts failing axially and its axial load decreases due to vertical load redistribution. Nonetheless, to the best of the authors' knowledge, the effect of axial load *increase* on the lateral response of R/C columns failing in shear has not yet been studied.

An experimental campaign is presented herein, aiming to shed further light on this phenomenon, i.e. the effect of vertical load redistribution on the non-linear response of shear- and flexure-shear-critical R/C columns neighboring failing vertical members. Six cantilever specimens were tested under quasi-static lateral cyclic load along with an axial load, which was either constant throughout the experiment or increased just before, or just after, the onset of shear failure. Two series of specimens were tested, one failing in flexure-shear and one predominantly in shear, all of them being short columns representative of older construction practice. Key test results are provided herein, along with an analysis of these results. Data from this study can be implemented in existing numerical models (e.g. [15,16]) to improve the modeling of shear and flexure-shear critical members and hence progressive collapse response of R/C buildings in general.

RESEARCH SIGNIFICANCE

Shear-critical columns in sub-standard R/C buildings may experience permanent increase of axial load due to the loss of bearing capacity of adjacent columns. This experimental study is the first one addressing the effect of axial load increase on the pre-peak and post-peak lateral response of shear-critical R/C columns. Its results can be used to enhance existing numerical models with the capability to accurately model failure of shear-critical column members and hence progressive collapse response of R/C buildings; such models are valuable in vulnerability analysis of old buildings for damage states close to collapse.

EXPERIMENTAL INVESTIGATION

Conceptual Design

Loss of axial load-bearing capacity of an R/C column leads to redistribution (through the horizontal members) of most of its vertical load to adjacent columns; this typically leads to a significant increase in the axial loads of the latter. Unlike the momentary fluctuations of axial load under earthquake loading, this increase is permanent and its effect should be clearly understood and modeled. To study the effect of axial load increase on the response of shear-dominated columns, shear-critical R/C column specimens were tested under cyclic lateral loading and increasing axial load. First, cyclic loading was applied along with constant axial load acting atop the specimen, simulating the conditions prior to vertical load redistribution. At some point, the vertical load was increased to the desired level and subsequently the lateral cycling resumed until reaching axial collapse. This procedure simulates the response to seismic loading of a column up to a certain point, redistribution of vertical loads due to axial failure of a neighboring column and continuation of the earthquake action up to vertical collapse of the first column.

Two series of specimens were fabricated, one failing in flexure-shear and another predominantly in shear. One column in each series is tested with constant axial load throughout the response to serve as reference. Table 1 presents the design details of each specimen. The focus is on older R/C construction lacking modern design and detailing rules, where column failure is not prevented by design.

A key parameter of the problem is the percentage of axial load increase. Usually, interior columns carry vertical loads of similar value and after axial failure of one of them, its load is redistributed to three or four columns around it. However, there are cases where higher load increase takes place, as when neighboring columns have different tributary areas. Based on these considerations, a 50% increase of the axial load is selected herein as a reasonably conservative value that may lead to a pronounced effect on the seismic response.

Another key parameter is the damage state at the instant of vertical load increase. In buildings struck by strong earthquakes there is substantial damage in most of the building before the loss of a column's vertical load bearing capacity, i.e. damage is not localized as in the case of e.g. blast loading; the extent of damage has a significant impact on the resulting response. For instance, an axial load increase at the early stages of pre-peak response might be beneficial for the overall response of the member, increasing its strength and stiffness, while the same axial load increase in the post-peak stage might prove detrimental. As the focus of this study is mainly on the peak and post-peak response, two different instants of axial load increase were selected to study its effect on the response. The first one is just before the onset of shear failure, and the second one immediately after it.

The aforementioned axial load increase intuitively seems likely to initiate at, or close to, the peak of a cycle of the displacement history. Nonetheless, according to previous shake-table tests (e.g. [17,18]), the loss of bearing capacity of a column and subsequent redistribution of

vertical loads takes place gradually over several load reversals. In the absence of a clearly defined "trigger point", the beginning of a cycle was chosen as the point of vertical load increase during the tests, mainly with the safety of the testing equipment in mind.

Test Specimens

Two sets of three columns with same geometry and materials but different reinforcement were designed and fabricated (Fig. 1); they were formed as cantilevers, representing the length between the base and the contraflexure point of short columns. The column cross-section is square, 300 × 300 (mm), and their length (at lateral loading level) is 715 mm (aspect ratio of 2.4). Consistent with old practice, the transverse reinforcement is sparse, Ø8/320 (mm) and Ø8/270 for the shear critical (SC) and flexure-shear critical (FSC) specimens, respectively, and has 90^o hooks (Fig. 1). The longitudinal reinforcement was designed to achieve the desired response and failure types; it is 12Ø16 (16 mm diam. bars) for the SC critical columns and 4Ø16+4Ø14 for the FSC columns resulting in a total reinforcement ratio of 2.68% and 1.58%, respectively.

The specimen design is shown in detail in Fig. 1, including the column mounting bases which were heavily reinforced to avoid any unwanted failure and make them sufficiently stiff, thus minimizing the displacement of the column top due to deformations of the base.

Materials

As per European Code[19], the concrete grade is C20/25 (characteristic cylinder strength of 20 MPa) and reinforcing steel grade is B500C (characteristic yield strength 500 MPa) for both the transverse and longitudinal reinforcement. Compression tests were performed on the same day as column tests. The measured strength was on average 27.7 MPa (individual specimen strengths shown in Table 1). Coupon tests on the ribbed reinforcement bars gave on average a yield stress of 565 MPa, tensile strength of 675 MPa and ultimate strain around 16%,.

Test set-up and instrumentation

Specimens are subjected to uniaxial bending and axial loading, as seen from the experimental set-up (Fig. 2). The double-acting double-hinged horizontal actuator applies a quasi-static cyclic load, operating in displacement-control mode, externally controlled by a dedicated displacement draw-wire sensor, since the standard actuator-based (internal) displacement-control may introduce significant 'lash' into the results, mainly due to the mounting setup and the non-negligible elastic deformations of the reaction frame, thus overestimating the actual lateral displacement of the tested specimens[20].

The loading protocol consisted of three cycles per displacement level with a step of 3.0 mm, typical of quasi-static cyclic tests (e.g. see ISO Displacement Schedule in [21]). Displacement histories are applied at constant rate, hence having longer duration at later stages; this rate is as low as 0.4 mm/s, to prevent development of noteworthy strain rate and inertial effects [21].

The double-hinged vertical actuator operates in force-control mode, dwelling at 180 kN, i.e. an axial load ratio (axial load over gross concrete cross-section axial capacity) of $v = 0.10$. Shortly before or soon after the onset of shear failure this load is increased to 270 kN, i.e. $v = 0.15$. A reference specimen in each set (FSC_1 and SC_1) is tested with constant axial load (180 kN). The axial load increase takes place within 9 s, corresponding to a load rate of 10 kN/s. This is done before the first cycle of 12 mm in FSC_2 and SC_2 and before the first cycle of 15 mm in FSC_3 and SC_3, as the onset of shear failure was found to occur at a displacement of 12 mm.

The instrumentation of the experiment comprises load cells, LVDTs, draw-wire sensors and strain gages. The load cells are mounted on the two actuators, measuring the resisting force from the specimens. Draw-wire sensors are used to measure the top lateral displacement, displacements along the diagonal needed to calculate shear deformations, and the potential base

uplift, in order to ensure that no significant base deformations develop. In the vertical direction, the axial deformation is directly measured from the axial displacement sensor of the vertical actuator. Strain gages were installed on longitudinal and transverse bars near the base of a shear-critical column (see detailed instrumentation arrangement in Fig. 3).

In addition to instrumental measurements, digital image correlation (DIC) was used to measure column deformations. Using a high-resolution camera from a fixed position, column images already painted with a speckle pattern were collected at each cycle. The distance between the initial and the shifted positions of each individual speckle point on the front face of the column can be measured at each cycle, providing the entire displacement contour along the front surface of each column throughout the duration of the test.

All recorded data is collected by the test controller at a frequency of 10 readings per second. Safety limits (displacements, forces) were imposed to automatically terminate the experiment, in case of structural imbalance.

TEST RESULTS AND DISCUSSION

Crack and Damage Propagation

Crack widths were measured using digital image correlation (details are given in [22]). The general pattern of damage initiation and propagation involves a horizontal crack forming very close to the column/base interface. Further horizontal cracks form higher up along the specimen at some distance from the interface crack and from each other, as a certain distance is required between cracks for the tensile strength to rebuild through bond. These cracks cross the position of the longitudinal bars, not extending much deeper into the specimen, and initiate quite early on, mostly at the displacement level of 3 mm (0.42% drift). The initial crack is usually wider than the subsequent cracks; all of them tend to increase in width with

increasing lateral displacement, while generally remaining stable or closing towards the last displacement cycles of the test. Moreover, fine diagonal and horizontal cracks appeared at the column/base joint at displacement levels of 6 mm and 9 mm, their width peaking at 12 mm (1.68% drift) (Fig. 4). The widest of these cracks reached a peak of about 0.35-0.45 mm. FSC specimens developed more flexural cracks in total along the height of the specimen – four to five – being affected more by flexure, while the SC ones developed two or three. Specimen SC_3's corner longitudinal bars were found to reach yield strain around the displacement levels of 9 to 12 mm and exceed it at 15 mm (2.10% drift).

Cross-inclined shear cracks appeared at a displacement level of approximately 6 mm (0.84% drift) or 9 mm (1.26% drift) and started opening considerably from about 12 mm (Fig. 4), reaching large widths of approximately 4 to 10 mm near the final cycles (Fig. 5). Their bottom end was always at the column/base interface and their inclinations were usually around 28^{o}-33^{o} on average. The SC specimens seem to have larger average shear crack angles than the FSC ones, which all exhibit 28^{o} angles on average. Spalling of concrete cover was observed close to the bottom ends of the inclined cracks, due to local decrease of the compression zone depths at those sections resulting from the shear cracks. Despite substantial opening of these diagonal cracks, no fracture of transverse bars occurred, as the 90^{o}-anchorage of the ties led to their slippage at high displacement levels. The strain gages mounted on transverse bars in SC_3 show that the tie at about 350 mm from the interface reached its strain-hardening branch at a displacement level of 15 mm (2.10% drift), developing very high strains afterwards. This is due to the opening of the full-depth crack at that point of the test, with the consequent opening of the gap. The tie placed about 30 mm above the interface did not yield, as it was not crossed by any shear crack.

Longitudinal bars of almost all specimens showed residual curvature due to buckling,

initiating near the end of the experiment. Their buckling length clearly exceeded the tie spacing, due to their 90^o hook and low anchorage length that do not provide adequate restraint. Moreover, disintegration of the concrete core was obvious, with parts of it having shattered during cycling, particularly near the last cycles.

Lateral Hysteretic Response

The specimens' hysteretic responses in terms of horizontal force (kN) vs lateral displacement (mm) or lateral drift (%) are shown in Fig. 6. Due to high sampling rate, smoothing has been applied to all hysteretic responses; original responses and smoothing method are given in [22].

The responses of the FSC (flexure-shear critical) specimens are quite similar, with peak strengths of around 150-160 kN developing at 12 mm (1.68% drift). Limited cyclic strength degradation and reloading stiffness degradation are exhibited in the pre-peak domain, which however increase significantly after peak.

The SC specimens remained almost 'elastic' up to a strength of around 130 kN (peak of the first displacement level), followed by a rather stiff strain-hardening branch up to about 200 kN at 12 mm displacement. One specimen (SC_3) did not reach its peak strength at a displacement of 12 mm (4^{th} cycle), but in the next cycle. This led to the increase in axial load occurring before the onset of shear failure, instead of just after it, as initially planned. The SC specimens also exhibit much higher cyclic strength degradation in the post-peak domain.

The highest cyclic strength degradation in each specimen takes place at the displacement level where the peak is reached, i.e. at the onset of shear failure. This coincides with the formation of a full-depth diagonal shear crack in each specimen (Fig. 4) in each loading direction and occurred in most specimens at a displacement of 12 mm (1.68% drift). In-cycle strength degradation, which in general was minor (recall that three cycles per displacement level were applied), was observed near the onset of shear failure in most specimens.

While the loops of both FSC and SC specimens are quite full at the first displacement levels, i.e. the specimens dissipate a large amount of energy (despite being shear critical), the loops become much thinner in the post-peak range. Pinching is observed in most responses, but is lower than expected given that the specimens are shear-critical. Of course, the 'low-stiffness' part of the response due to closing of cracks of one side and reopening of the other side's cracks upon reversal is observed, especially near the final cycles.

The displacement capacities of the specimens vary substantially; SC specimens reach higher displacements in absolute terms than the FSC ones, largely due to higher longitudinal reinforcement content, which leads to higher post-peak displacements[15]. Attained displacement ductilities are compared in Table 2 at peak strength (i.e. onset of shear failure), at the maximum attained displacement and (wherever applicable) at the onset of axial failure. The yield displacement is taken for convenience as the displacement on the cyclic envelope curve corresponding to a strength equal to 70% of the peak strength. The displacement ductility achieved by most specimens (notwithstanding the definition of yield point) is remarkable given their poor design and their shear-dominated response – usually characterized as 'non-ductile' or even 'brittle'. All of them reach their peak resistance at a ductility between 4 and 6 (drifts between 1.7% and 2.1%). The specimens that do fail axially reach a ductility of 6.5 to 7.5 (drifts between 2.1% and 2.9%), while the specimens that do not fail axially are shown to exceed a ductility of 10 (drifts between 2.9% and 3.8%), far more than would normally be expected from such designs.

Axial Response

The average (over the section) vertical displacements at the top of the specimen (mm) vs. lateral displacements (mm) are presented in Fig. 7. Since the recording system was reset after the axial load was applied, the vertical displacement at the initial position is taken as 0.0 mm;

in reality, it is lower and was estimated based on the specimens' properties as 0.048 mm. Vertical displacements of all specimens follow the typical U-shaped pattern up to the onset of shear failure, i.e. having a specific negative displacement (compressive strain) at the 'vertical' position (zero lateral displacement) with increasing displacements towards the peaks of each cycle. The increased vertical displacements at the extremes of each cycle come from the well-known phenomenon of member elongation in the nonlinear range of the response; curvatures lead to high tensile strains of the tension reinforcement, also accompanied by opening of cracks; with consecutive cycles at increasing lateral displacements, plastic strains accumulate leading to further elongation.

However, the shape of the observed pattern changes from the onset of shear failure onwards; from a U-shape, it turns flat and eventually into an inverted-U-shape, while vertical displacements generally decrease further with each cycle. This corresponds to a change in the physical behavior of a member; as the peak of each cycle is reached after the full depth diagonal crack has formed, the upper discrete parts of the column are pushed downwards under the influence of the constant axial load. Of course, as the displacement reverses, the cracks partly close and a part of this downward displacement is recovered (hence the inverted-U-shape); after a given point, the accumulation of downward displacements becomes very significant with vertical displacements decreasing to even less than -5 mm (i.e. an average normal strain of -0.7%). The sudden increase of axial deformations accompanying the onset of axial failure is shown to start at around -7 mm for this test series. Specimens FSC_2, FSC_3 and SC_2 exhibited this behavior, while FSC_1, SC_1 and SC_3 were stopped before the onset of axial failure either for the safety of the equipment or because the specimen was observed to have been damaged extensively and its resistance had fallen to a small fraction of the previously attained maximum strength.

Effect of Vertical Load Increase

It is clear in both experimental series that specimens with an axial load increase before the peak strength (namely FSC_2, SC_2 and SC_3) reach a higher strength than the ones with constant axial load. This was expected, as higher compression loads increase shear strength, so long as failure is caused by diagonal tension. This increase is about 3-4%, rather shy of the predictions of 4-8% based on existing shear models [23–26] for an axial load increase of 50%. Fig. 8a shows the descending branch slope values estimated from the envelopes of the experimental loops. It is clear that increasing the axial load leads to higher degradation rate in the post-peak range. In all specimens with increasing axial load the descending branches are steeper than in the constant load ones; only FSC_2 is almost equal to FSC_1, most likely due to the higher concrete strength, partly compensating for the increased applied axial load. The maximum horizontal displacement attained by each specimen is presented in Fig. 8b with specimens that failed axially having a gradient filling; note that this is a lower bound of deformability for the ones that did not fail axially. FSC_1 with low constant axial load is cycled up to 21 mm (2.94% drift) without losing its vertical load-bearing capacity. FSC_2 and FSC_3 (specimens with increased axial load) fail well before that, reaching a lateral displacement at the onset of axial failure of 18 mm (2.52% drift) and 15 mm (2.10% drift), respectively. In this series, increasing the load after the peak is reached led to the axial capacity being lost sooner than increasing it before the peak. In the SC series, the axial load in both specimens (SC_2 and SC_3) was increased before the peak, due to SC_3's unexpected higher displacement at onset of shear failure (compared to all other specimens). SC_2 had lower deformability than SC_1, i.e. 21 mm (2.94% drift) instead of 27 mm (3.78% drift), while SC_3 achieved the same displacement as SC_1 whose axial load was kept constant, being however much closer to axial failure than the reference specimen, reaching a

vertical displacement of 5.6 mm as contrasted to the 2.8 mm of SC_1. Judging from the trend of vertical responses, SC_3 would fail axially before completing the three 27 mm (3.78% drift) cycles, while SC_1 managed to complete all of them without nearing axial failure.

Strength prediction

Yield and ultimate moments were calculated from moment vs. curvature (M-φ) analysis using the RCCOLA.NET[27] software. Shear strength was calculated based on four models[23–26] predicting the maximum resistance, i.e. before shear strength degradation due to increasing inelastic flexural deformations starts (Table 3); Priestley[23] model's predictions are presented for shear crack angles of both 30° and 45°. The Eurocode 8-3[25] equation is applied with mean material values, without safety factors, and with displacement ductility $\mu_{\Delta,pl}$ and compression zone depth corresponding to yielding. For the *fib* Model Code 2010[26] equation, safety factors are disregarded and it is based on a level III approximation (a rather detailed approach).

Comparing the predicted with the experimentally recorded strengths, one can see that the FSC specimens exceeded the predicted ultimate flexural strength, perhaps due to discrepancies between the modeled and actual steel yield strength, steel hardening and concrete strength. On the other hand, the SC specimens are controlled by shear strength. It is clear from Table 3 that the prediction of the maximum shear resistance of an R/C element is subject to significant variability, mostly deriving from different weighting of the influence of various column properties on shear strength. The Priestley model[23] and the Eurocode 8-3[25] equations seem to predict the SC specimens' shear strength well, while the rest underestimate it. The FSC specimens' shear strength is underestimated by all models except Priestley's[23] that overestimates it, especially when the recommended strut angle (30°) is used.

Deformation Analysis

Specimen deformations were calculated based on displacement sensors (LVDTs) and Digital

Image Correlation (details in [22]). It is observed (Fig. 9) that shear-induced displacements always start off low, around 10-15% of the total displacement, at a displacement level of 3 mm (0.42% drift). They increase steadily as damage propagates and much more sharply from the onset of shear failure onwards. They reach percentages of 40 to 70% at the final displacement levels. Conversely, the flexural (also including bond-slip) displacements start as a high proportion of the total, around 85-90%. Although they increase considerably in subsequent cycles in absolute terms, they decrease as a percentage of the total displacement up to the onset of shear failure. After the onset of shear failure, flexural and bond-slip displacements either remain constant or decrease in absolute values leading to significant further decrease in their relative contributions to the total displacements up to axial failure. These findings clearly indicate the predominance of shear mechanisms after peak strength. FSC specimens have higher percentages of flexural displacements than the SC specimens. This observation, combined with the fact that in FSC specimens more flexural cracks form, are clear indications of the higher influence of flexure in these specimens than in the SC ones.

Lateral stiffness degradation

The secant stiffness at peaks of the hysteretic response is presented in Fig. 10 for representative specimens of each set, taking into account the average of positive and negative directions. Overall, stiffness degradation is similar in all specimens with few discrepancies. There is a very significant decrease in stiffness with increasing ductility, the stiffness decreasing by about 50% from the 3 to the 6 or 9 mm displacement.; thereafter, it keeps decreasing, reaching zero stiffness asymptotically after 18 mm (2.52% drift). The second and third cycles have only slightly lower stiffness than the first cycles at initial displacement levels. From 9 or 12 mm (1.26% to 1.68% drift), the difference becomes larger, due to higher cyclic strength and reloading stiffness degradation. The elastic (gross) flexural stiffness,

assuming a cantilever of 715 mm length, 20 MPa concrete and 300 × 300 cross-section, would be 166 kN/mm. Nonetheless, the measured stiffness at the first peak of the first displacement level is found to be considerably lower, roughly 25% of that value. An important source of the difference from the estimated elastic flexural stiffness is that at 3 mm flexural cracking has already started, while early shrinkage cracking is also contributing to stiffness reduction; as seen in the hysteresis loops (Fig. 6), the first cycle by no means corresponds to a linear elastic response. At the same time, shear deformations were found to be a noticeable fraction of the total lateral displacement at this stage (Fig. 9), about 10 to 15%. Other possible minor sources of discrepancy are bending of the plates connecting the actuator to the column, as well as some added flexibility from the deformation of the specimen base. It cannot be known exactly to what extend each factor influences the recorded value, but flexural cracking and shear deformations are considered the principal sources.

Energy dissipation

SC specimens are found to cumulatively dissipate more energy than the FSC ones in absolute terms, primarily due to the significantly higher strength owing to a higher longitudinal reinforcement ratio and the difference with regard to the attained ultimate displacement. Nonetheless, when normalized by their respective strength (Fig. 11), FSC specimens seem to be dissipating more energy than the SC ones at any given displacement, which is in line with what would be expected from specimens with a more ductile (FSC) as opposed to a more brittle (SC) behavior. The rate of energy dissipation is found to increase considerably after 6 mm (0.84% drift), when plastic deformations increase significantly. They tend to slightly decrease again after 21 mm (2.94% drift), due to the drastic strength and stiffness degradation, leading to very pinched hysteresis loops.

SUMMARY AND CONCLUSIONS

The experimental program presented herein sheds more light on the non-linear response of shear-critical and flexure-shear-critical R/C columns, addressing for the first time the effect of axial load increase (triggered by loss of axial load capacity of neighboring columns). Six cantilever specimens (three flexure-shear and three shear critical), representative of older construction, were tested under a quasi-static cyclic lateral loading, having their axial load increased just before or after the onset of shear failure.

Both specimen sets exhibited relatively similar hysteretic response, with limited cyclic degradation in the pre-peak domain that increases significantly post-peak, and remarkable displacement ductility. Shear critical specimens attained higher strength and displacement, owing to their considerably higher longitudinal reinforcement.

All specimens initially developed horizontal flexural cracks , which kept opening up to about the onset of shear failure, remaining stable or closing thereafter. These were followed by cross-inclined shear cracks that appeared before the onset of shear failure, turned into full-depth cracks at the peak and kept opening substantially with increasing displacement post-peak, accompanied by slippage and opening of the insufficiently anchored ties. Following the typical for shear failure transition of axial deformations from a U-shape to an inverted U-shape, a sudden increase in downward displacement, with a corresponding drop of axial load resistance, signaled the onset of axial failure.

Deformation decomposition showed a clear trend of increasing shear deformations with increasing displacement in all specimens, which became much more pronounced after the onset of shear failure, accompanied by retraction of flexural and bond-slip deformations. Between half and two thirds of the total deformations were attributed to shear by the end of

all tests. Flexure-shear critical specimens exhibited higher percentages of flexural and bond-slip displacements than shear critical specimens throughout the test, as well as more moderate increase of shear deformations post-peak.

The increased axial load just before or after the onset of shear failure was found to adversely affect the post-peak response of sub-standard R/C members. It led to higher rate of post-peak shear strength degradation and lower displacement at onset of axial failure of shear-damaged R/C columns – accompanied by comensurate reduction in total dissipated energy. On the other hand, it didn't seem to have any considerable impact on the energy dissipation capacity or lateral stiffness degradation of the members of this test series. Further experimental studies are necessary to establish clear patterns with regard to the amount of axial load increase and to the instant of axial load increase. No clear difference between the application of the load before or after the peak could be detected, as there were only three and one such specimens, respectively. More experimental studies should be performed with a broad range of design characteristics, initial axial loads, increased/decreased axial loads and points of axial load change, to improve the prediction of the impact of axial load change on the non-linear hysteretic response of sub-standard RC columns and be able to comprehensively model and assess sub-standard R/C frame buildings.

ACKNOWLEDGMENTS

The authors would like to sincerely thank all the staff of the Laboratory of R/C and Masonry Structures, AUTh, where this experimental study was carried out. The first author would also like to gratefully acknowledge the support provided by City, University of London to carry out the experiments as part of his doctoral degree scholarship and Basler & Hofmann AG for the support during the write-up of this research work.

REFERENCES

1. Sezen, H. and Moehle, J., "Seismic Tests of Concrete Columns with Light Transverse Reinforcement," *ACI Structural Journal*, V. 103, No. 6, 2006, pp. 842–849.

2. Ghannoum, W. M., Moehle, J. P. and Bozorgnia, Y., "Analytical Collapse Study of Lightly Confined Reinforced Concrete Frames Subjected to Northridge Earthquake Ground Motions," *Journal of Earthquake Engineering*, V. 12, No. 7, 2008, pp. 1105–1119.

3. Lodhi, M., "Seismic Evaluation of Reinforced Concrete Columns and Collapse of Buildings," PhD Thesis, The Ohio State University, 2012.

4. Sasani, M., Bazan, M. and Sagiroglu, S., "Experimental and Analytical Progressive Collapse Evaluation of Actual Reinforced Concrete Structure," *ACI Structural Journal*, V. 104, No. 6, 2007, pp. 731–739.

5. Izzuddin, B. A., Vlassis, A. G., Elghazouli, A. Y. and Nethercot, D. A., "Progressive Collapse of Multi-Storey Buildings due to Sudden Column Loss – Part I: Simplified Assessment Framework," *Engineering Structures*, V. 30, No. 5, 2008, pp. 1308–1318.

6. Yu, J. and Tan, K. H., "Experimental and Numerical Investigation on Progressive Collapse Resistance of Reinforced Concrete Beam Column Sub-Assemblages," *Engineering Structures*, V. 55, 2013, pp. 90–106.

7. Lew, H. S., Bao, Y., Pujol, S. and Sozen, M. A., "Experimental Study of Reinforced Concrete Assemblies under Column Removal Scenario," *ACI Structural Journal*, V. 111, No. 4, 2014, pp. 881–892.

8. GSA (General Services Administration), "Alternate Path Analysis and Design Guidelines for Progressive Collapse Resistance," 2013, 143 pp.

9. Xu, G. and Ellingwood, B. R., "An Energy-Based Partial Pushdown Analysis Procedure for

Assessment of Disproportionate Collapse Potential," *Journal of Constructional Steel Research*, V. 67, No. 3, 2011, pp. 547–555.

10. Murray, J. A. and Sasani, M., "Seismic Shear-Axial Failure of Reinforced Concrete Columns vs . System Level Structural Collapse," *Engineering Failure Analysis*, V. 32, 2013, pp. 382–401 .

11. Lynn, A. C., Moehle, J. P., Mahin, S. A. and Holmes, W. T., "Seismic Evaluation of Existing Reinforced Concrete Building Columns," *Earthquake Spectra*, V. 12, No. 4, 1996, pp. 715–739.

12. Ousalem, H., Kabeyasawa, T., Tasai, A. and Ohsugi, Y., "Experimental Study on Seismic Behavior of Reinforced Concrete Columns under Constant and Variable Axial Loadings," *Proceedings of the Japan Concrete Institute*, V. 24, No. 2, 2002, pp. 229–234.

13. Ramirez, H. and Jirsa, J., "Effect of Axial Load on Shear Behavior of Short RC Columns under Cyclic Lateral Deformations," PMFSEL Report No. 80-1, 1980, 205 pp.

14. Nakamura, T. and Yoshimura, M., "Gravity Load Collapse of Reinforced Concrete Columns with Decreased Axial Load," *2nd European Conference on Earthquake Engineering and Seismology*, 2014.

15. Zimos, D. K., Mergos, P. E. and Kappos, A. J., "Modelling of R/C members accounting for shear failure localisation: Hysteretic shear model," Earthquake Engineering & Structural Dynamics, V. 47, No. 8, 2018, pp. 1722–1741.

16. Zimos, D. K., Mergos, P. E. and Kappos, A. J., "Modelling of R/C members accounting for shear failure localisation: Finite element model and verification," Earthquake Engineering & Structural Dynamics, V. 47, No. 7, 2018, pp. 1631–1650.

17. Elwood, K. and Moehle, J. P., "Shake Table Tests and Analytical Studies on the Gravity Load Collapse of Reinforced Concrete Frames," PEER 2003/01 364, 2003.

18. Ghannoum, W. and Moehle, J., "Shake-Table Tests of a Concrete Frame Sustaining Column Axial Failures," *ACI Structural Journal*, V. 109, 2012, pp. 393–403 .

19. European Committee for Standardization (CEN), "Eurocode 2. Design of concrete structures. Part 1-1: General rules and rules for buildings," EN 1992-1-1, 2004.

20. Pilitsis, V. G., Papanikolaou, V. K., Tegos, I. A. and Stylianidis, K. A., "A Novel Mechanism for Restraining Seismic Actions in Ductile Bridges: Analytical Modeling and Experimental Verification," *COMPDYN 2015 Computational Methods in Structural Dynamics and Earthquake Engineering*, Crete Island, Greece, 2015, 14 pp.

21. ASTM International, "Standard Test Methods for Cyclic (Reversed) Load Test for Shear Resistance of Vertical Elements of the Lateral Force Resisting Systems for Buildings," Report ASTM E2126-11, West Conshohocken, PA, 2011.

22. Zimos, D. K., "Modelling the Post-Peak Response of Existing Reinforced Concrete Frame Structures Subjected to Seismic Loading," PhD Thesis, City, University of London, 2017: openaccess.city.ac.uk/18531/

23. Priestley, M., Verma, R. and Xiao, Y., "Seismic shear strength of reinforced concrete columns," *Journal of Structural Engineering*, V. 120, 1994, No. 8, pp. 2310–2329.

24. Sezen, H. and Moehle, J., "Shear strength model for lightly reinforced concrete columns," *Journal of Structural Engineering*, V. 130, No. 11, 2004, pp. 1692–1703.

25. European Committee for Standardization (CEN), "Eurocode 8. Design of structures for earthquake resistance. Part 3: Assessment and retrofitting of buildings," EN 1998-3, 2005.

26. International Federation for Structural Concrete (fib), "Model Code 2010: First Complete Draft," 2010.

27. Kappos, A. J. and Panagopoulos, G., "RCCOLA-NET: A computer program for the analysis of the inelastic response of reinforced concrete sections," Laboratory of Reinforced

Concrete and Masonry Structures, Department of Civil Engineering, Aristotle University of Thessaloniki, 2011.

Table 1 – Details of column specimens

Specimen	Failure mode	Axial load (kN)	Point of axial load increase	Concrete Strength (MPa)	Transverse reinforcement	Longitudinal reinforcement
SC_1	Shear	180	-	32.8	Ø8/320	12Ø16
SC_2	Shear	180 → 270	before 1st cycle 12 mm	27.2	Ø8/320	12Ø16
SC_3	Shear	180 → 270	before 1st cycle 15 mm	24.3	Ø8/320	12Ø16
FSC_1	Flexure-Shear	180	-	26.0	Ø8/270	4Ø16+4Ø14
FSC_2	Flexure-Shear	180 → 270	before 1st cycle 12 mm	28.3	Ø8/270	4Ø16+4Ø14
FSC_3	Flexure-Shear	180 → 270	before 1st cycle 12 mm	27.7	Ø8/270	4Ø16+4Ø14

Table 2 – Displacement ductilities of specimens at various levels

Specimen	μ_{peak}	$drift_{peak}$ (%)	μ_{max}	$drift_{max}$ (%)
FSC_1	6.0	1.7	10.5	2.9
FSC_2	4.3	1.7	6.4	2.5
FSC_3	5.5	1.7	7.0	2.1
SC_1	4.6	1.7	10.4	3.8
SC_2	4.3	1.7	7.5	2.9
SC_3	5.7	2.1	10.3	3.8

Table 3 – Maximum experimentally recorded strength and predicted flexure- and shear-controlled resistances (kN).

Specimen series:			*SC*	*FSC*
Shear at flexural strength (*from M-φ* analysis)		**Yield**	198	141
		Ultimate	204	146
Predicted Shear strength	**Priestley *et al.***	**30º**	198	211
		45º	171	179
	EC8-3		198	143
	Sezen & Moehle		134	142
	MC2010		137	143
Maximum shear measured in tests			183	161

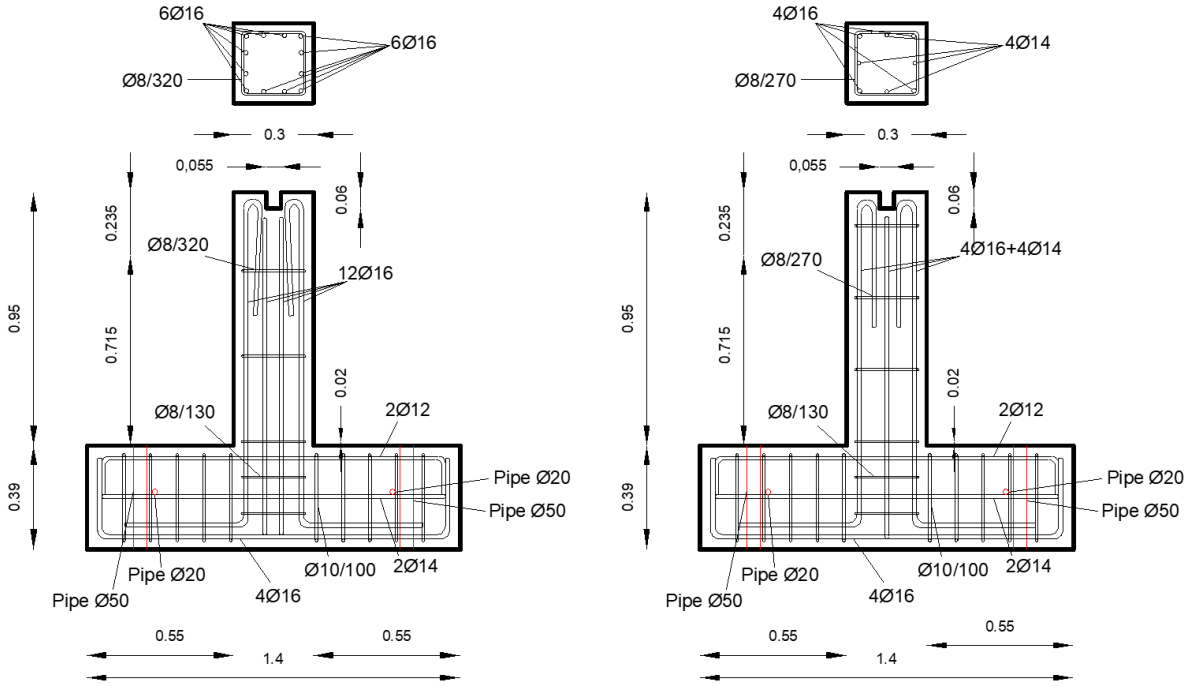

Fig. 1: Design of (a) shear critical (SC) and (b) flexure-shear critical (FSC) specimens (lengths in m; rebar and pipe diameters in mm).

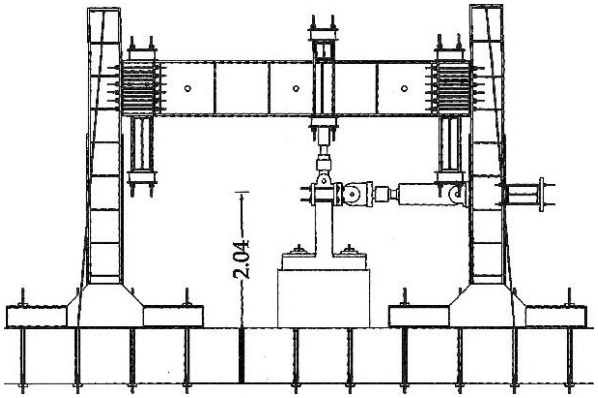

Fig. 2: Experimental set-up shown schematically.

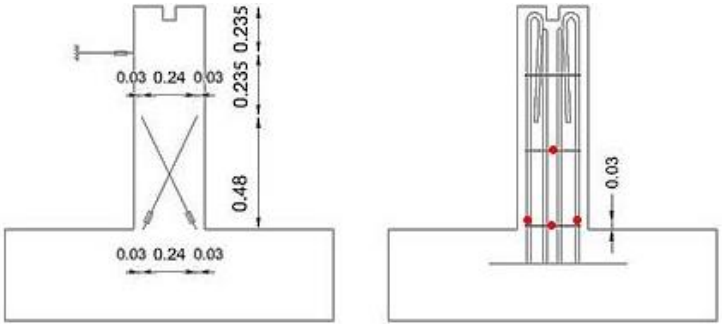

(a) (b)

Fig. 3: Instrumentation of specimens: (a) draw-wire sensors and (b) strain gages.

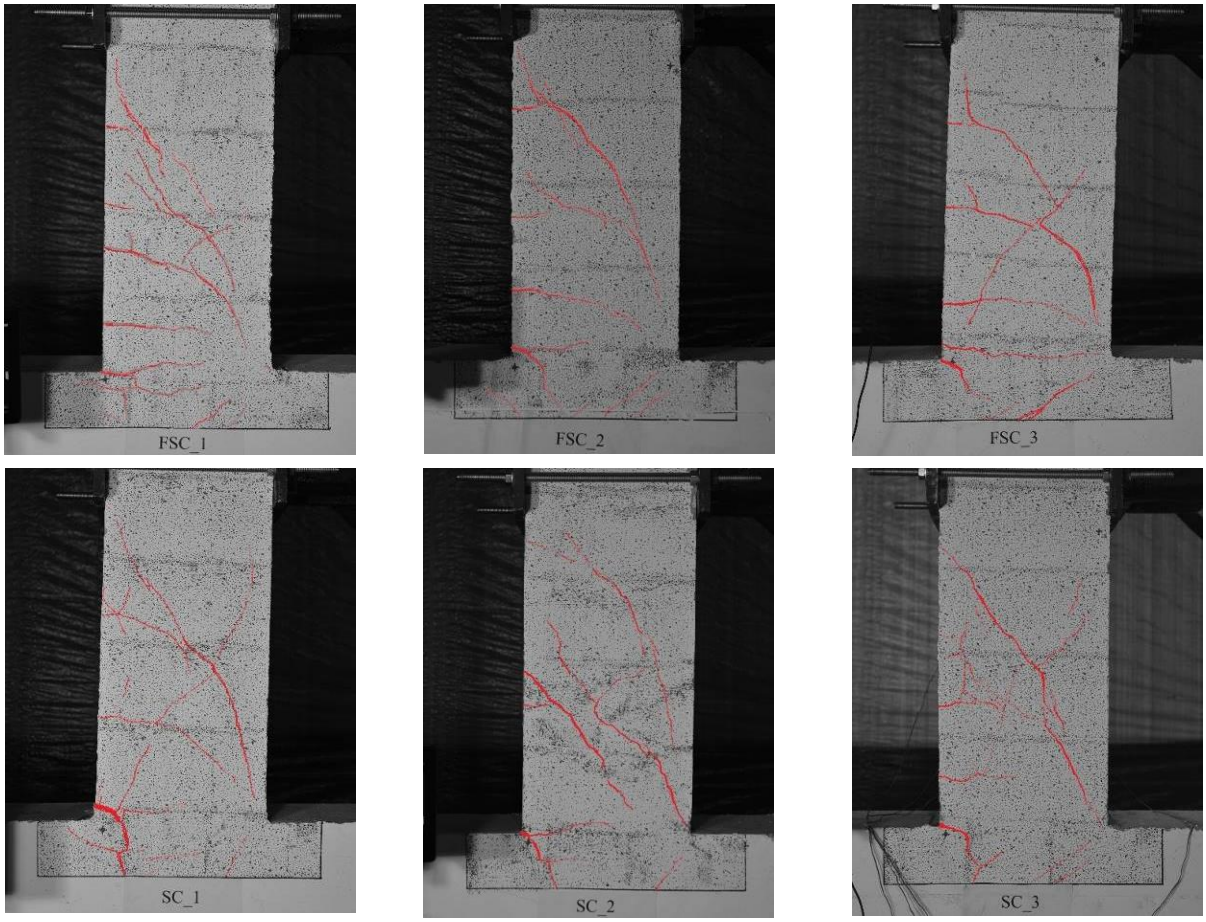

Fig. 4: Damage state (surface crack patterns) of specimens at displacement level of 12 mm.

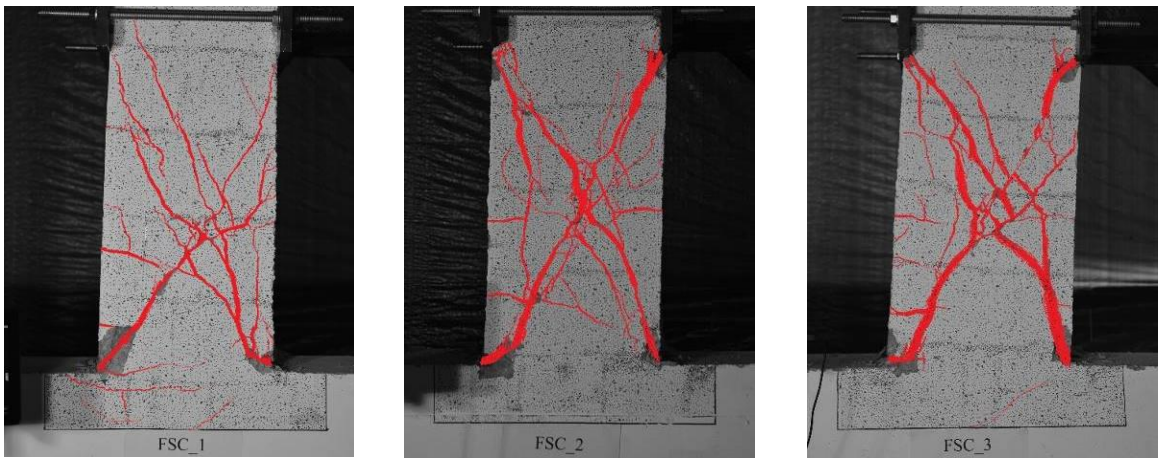

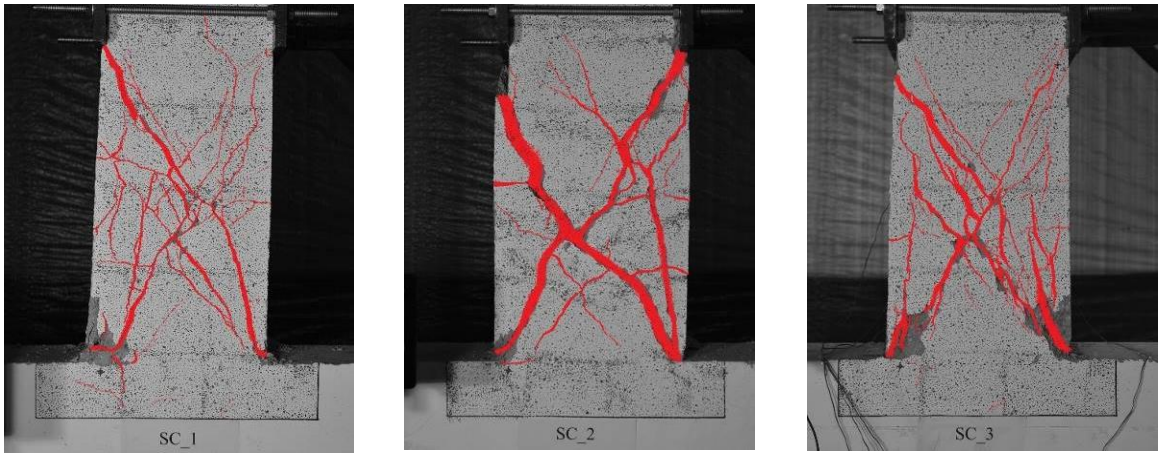

Fig. 5: Damage state (surface crack patterns) of specimens at displacement level of 18 mm (15 mm for FSC_3).

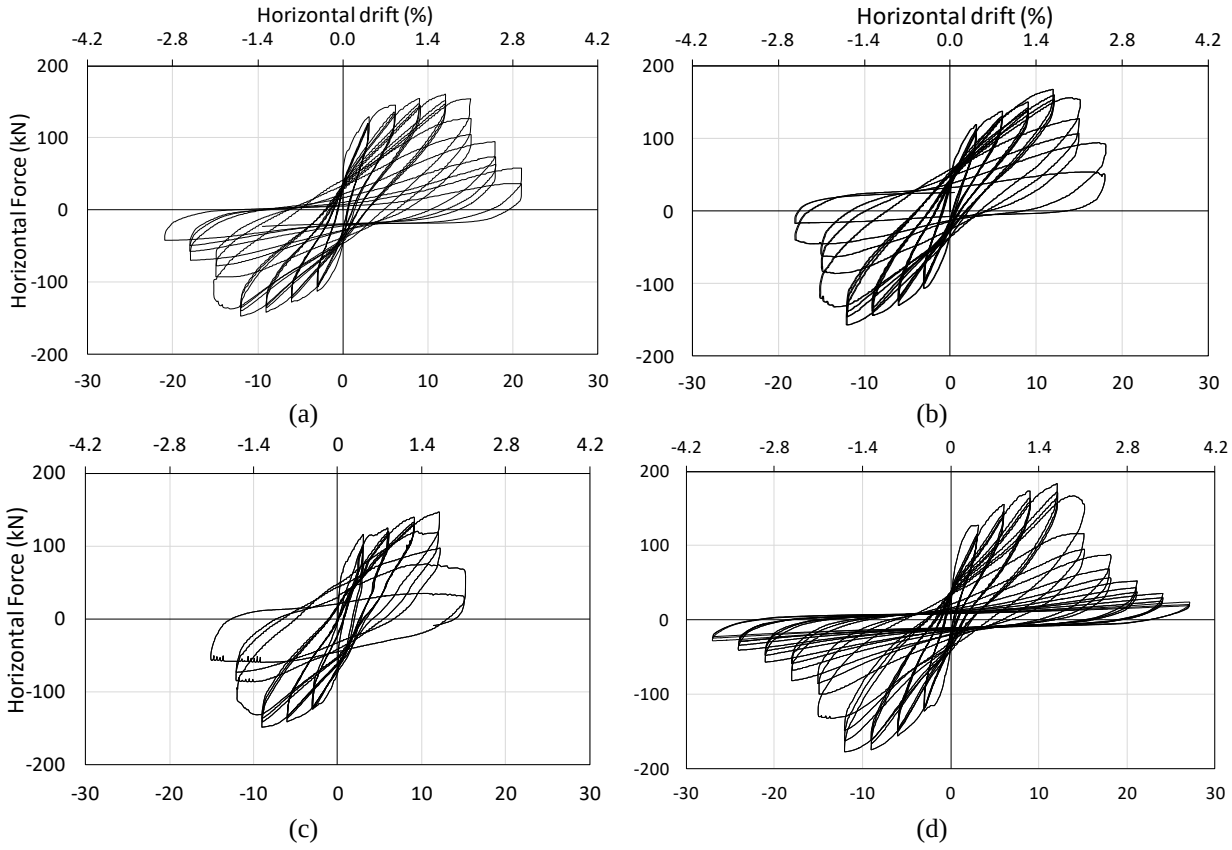

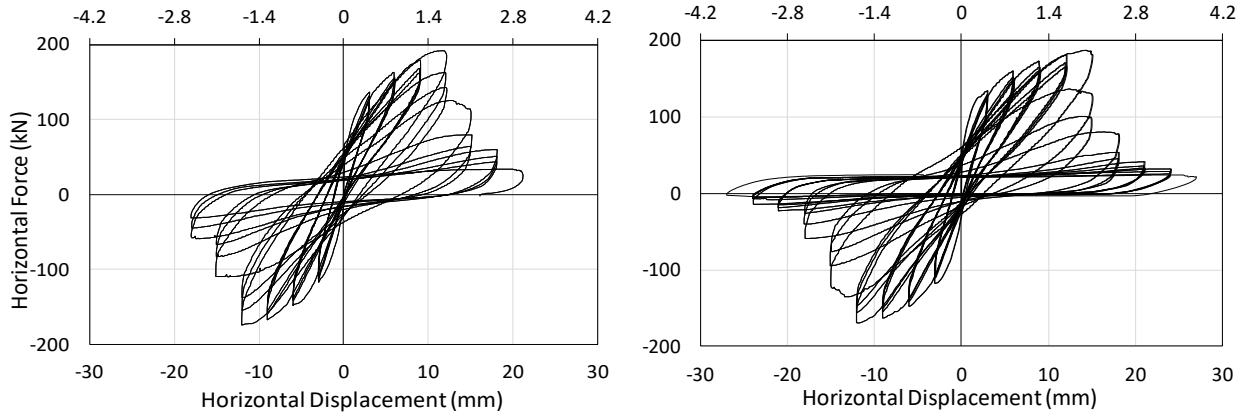

(e) (f)

Fig. 6: Hysteretic response of specimens (a) FSC_1, (b) FSC_2, (c) FSC_3, (d) SC_1, (e) SC_2 and (f) SC_3.

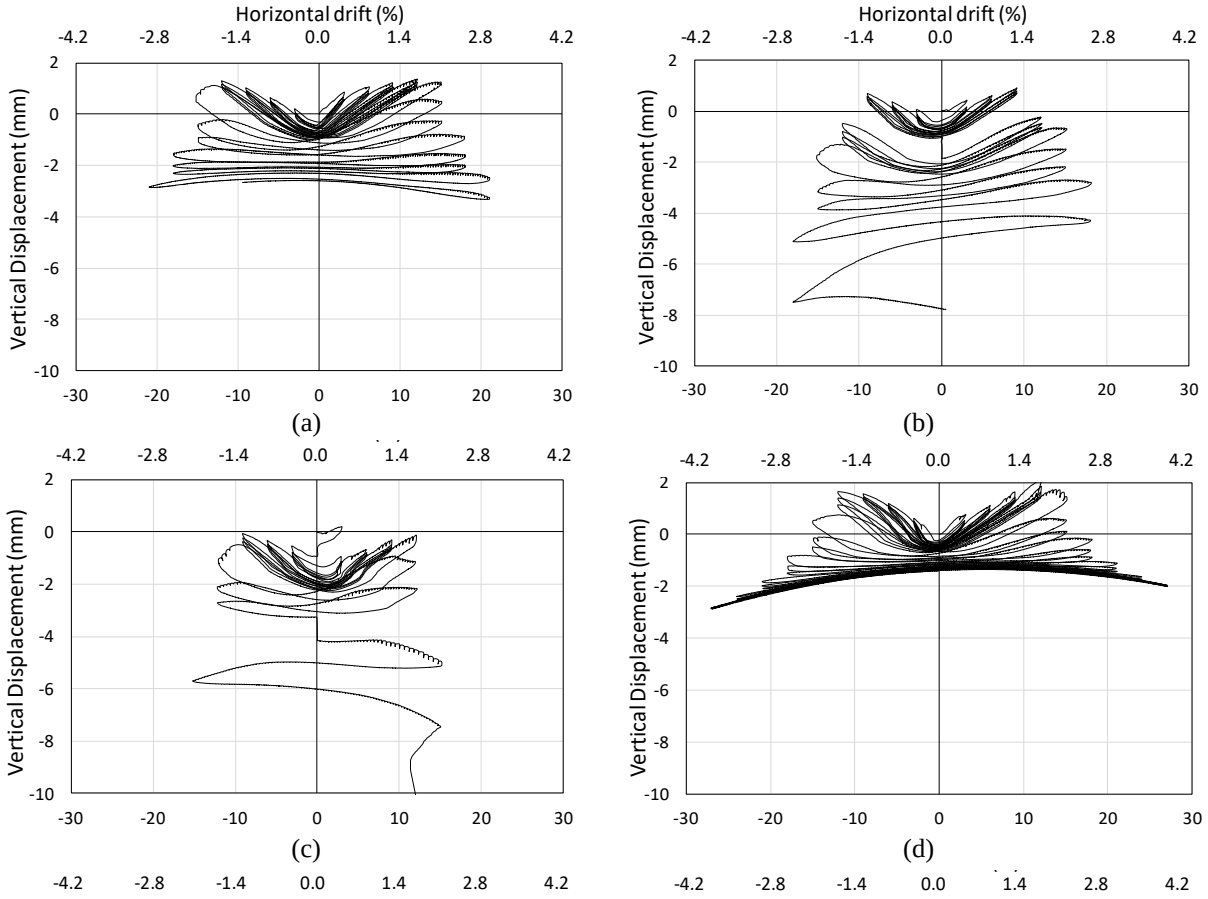

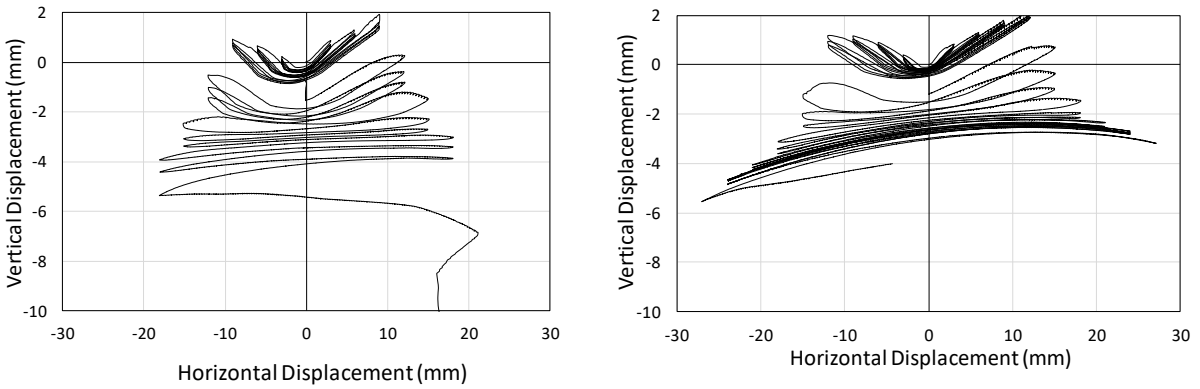

(e) (f)

Fig. 7: Axial hysteretic response of specimens (a) FSC_1, (b) FSC_2, (c) FSC_3, (d) SC_1, (e) SC_2 and (f) SC_3.

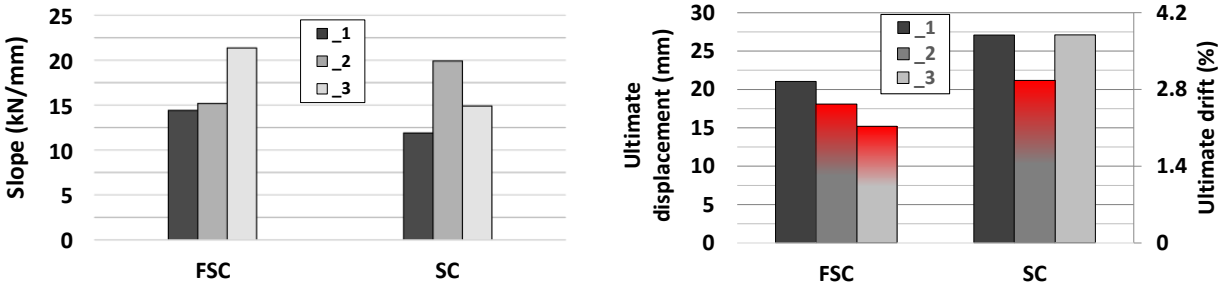

(a) (b)

Fig. 8: (a) Experimentally obtained descending branch slopes, and (b) maximum horizontal displacements of FSC and SC specimens.

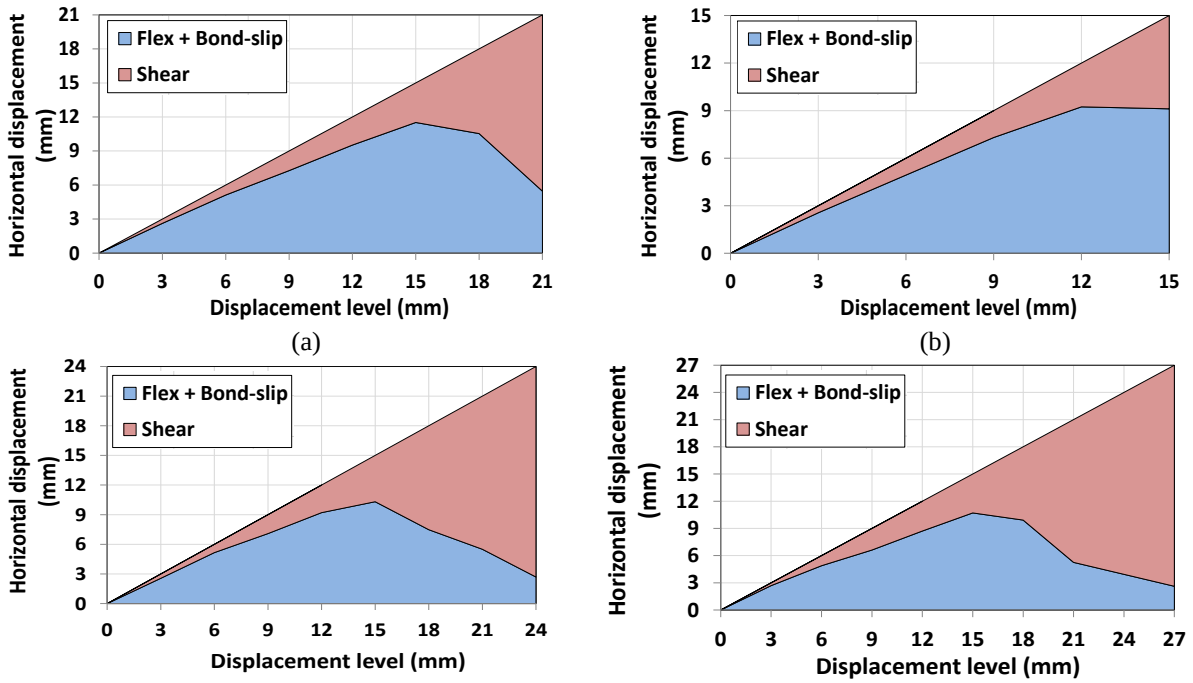

(a) (b)

(c) (d)

Fig. 9: Lateral displacement decomposition: (a) FSC_1, (b) FSC_3, (c) SC_1, and (d) SC_3.

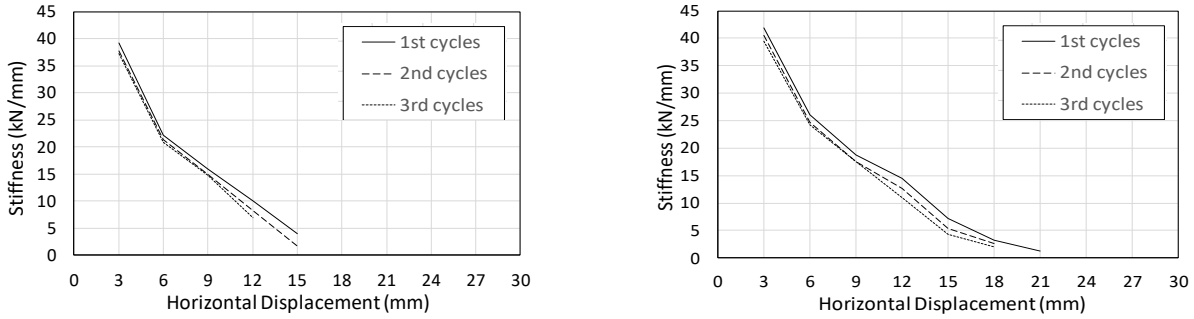

Fig. 10: Lateral displacement secant stiffness against attained lateral displacement for (a) FSC_3, and (b) SC_2.

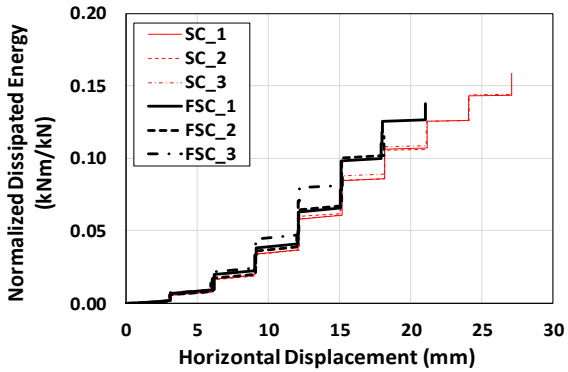

Fig. 11: Cumulative dissipated energy normalized to recorded strength vs. displacement level for all specimens.

TABLES AND FIGURES

List of Tables:

List of Figures: